Acta Polytechnica **64**(5):470–486, 2024
https://doi.org/10.14311/AP.2024.64.0470

Published by the Czech Technical University in Prague

ACOUSTIC RADIATION BEAM PATTERNS OF DIFFERENT POLYGONAL PISTON SURFACES

Taofeek Ayotunde Yusuf[a,*], Sheriff Abiodun Aodu[b], Abeeb Opeyemi Alabi[b]

[a] *Joseph Sarwuan Tarka University, Mechanical Engineering Department, P. M. B. 2373, 970101 Makurdi, Nigeria*

[b] *Kyungpook National University, School of Mechanical Engineering, Daehak-ro 80, 41566 Daegu, South Korea*

[*] corresponding author: yustaofeekay@yahoo.com

Abstract. Transducers are used in acoustic remote sensing and several other modern applications. The radiating surface geometry of a single acoustic transducer affects its beam pattern and has a cumulative effect on the overall performance of an array configuration. In addition, the transducers with polygon radiating surfaces provide more compact structure in an array than the circular pistons due to their flat surface edges. However, until now, the radiation patterns of acoustic polygonal pistons have not been exclusively studied and documented. In this study, the directional factors of acoustic pistons with polygonal surfaces of three to ten sides were derived analytically from the first principle using the Rayleigh integral. These directional factors were used to synthesise and characterise the radiation patterns of the piston sources in comparison with the baffled circular piston of an equivalent surface area. The rectangular, the triangular, and the rest of the polygons have the same performance with the circular piston when the surface diameter is not higher than 0.5λ, 0.28λ and 0.43λ, respectively. The main lobe of the acoustic emissions from the square is very close to that of the circular piston whose diameter is greater than a wavelength while that of the rectangle is wider. The results show that the radiating surface perimeter and symmetry are the two most critical factors affecting the beam characteristics of a piston source rather than the surface area or the number of sides. The theoretical results were validated using the finite element method with an excellent compliance.

Keywords: Polygonal piston source, acoustic transducer, Rayleigh integral, radiation beam, finite element analysis.

1. Introduction

The acoustic transducer technology is relevant in many areas of contemporary applications, such as underwater sonar [1], biomedical diagnosis [2], fluid flow and heat transfers [3], energy harvesting [4], non-destructive testing [5], and enhanced oil recovery [6]. In underwater applications, acoustic transducers are used as sensors through the technology of transmission of sound waves for the purpose of remote communication, imaging, or detection [7, 8]. One of the output characteristics for determining the performance of such devices is a beam pattern. The beam pattern is a logarithmic function (decibel scale) of an angle-dependent characteristic called the directivity factor. The directional factor is strongly influenced by the combined effect of the area of its radiating surface and the frequency of operation. This makes the geometric dimensions of an acoustic element a critical aspect of an effective design [9]. In addition, the surface geometry of individual component transducer elements affects both the overall performance and the optimisation of inter-element spacing in an array transducer structure.

For the beam pattern synthesis, a single transducer is considered as an elastic membrane vibrating like an acoustic piston. The directional factor of a circular piston on a rigid infinite baffle is well known and has been used in several studies [10–16]. However, circular pistons are unsuitable for composing an array transducer of densely packed elements. They typically leave inevitable gaps between their edges contributing to poor space conservation [17, 18] and a considerable loss in the radiated power [19]. Meanwhile, acoustic pistons with flat surfaces such as polygons have more prospects in providing a more compact transducer structure [20]. In addition, their side lengths can be varied independently to increase the radiating surface area without increasing the size in all the directions. This offers a more efficient way to control the overall size of the transducer than using the circular pistons without the liability of an added cost [21]. While the square and rectangular pistons are also being fairly used in few instances [22, 23], the higher-sided polygons such as the hexagon have more elements in their primary neighbourhood, which enhances their radiation characteristics in a staggered array configuration [20].

To date, there has been no independent study that has exclusively analysed these polygonal surfaces and effectively characterised their acoustic radiation performance. Roh et al. made an effort in that direction but apparently made no distinction between the rectangular and square sources while some weird non-symmetrical geometries, such as the triangle and pentagon, were not included [19]. Consequently, this study took a more comprehensive approach on this subject. The directional factors of nine (9) acoustic pistons sources having 3–10 sided polygon surfaces were characterised and compared with that of the circular piston on a rigid baffle, which was used as the standard. Using the finite element commercial software, Pzflex®, Tonpilz transducer structures were modelled and simulated using the geometries of the piston sources for the shapes of the head masses to validate the theoretical results. The comparison between the theoretical and FEM beam patterns showed good agreements. Finally, the expression for the directional factors were standardised to facilitate their adoption in subsequent designs.

2. Equivalent surface area of the piston sources

The circular piston of a given radius ac is used as the standard reference as shown in Figure 1. Figure 2 shows the polygonal pistons with three to ten surfaces proposed for this study, respectively. The half-side length (HSL) a of each of them carries the subscripts denoting the first letter of their respective names except for the hexagon defined as a_x in Figure 2e. All the polygons are regular except the rectangle where one side is equal to the diameter of the circular piston as shown in Figure 2b.

The diameter of the circular surface is specified in terms of the wavelength λ that was calculated using $\lambda = \frac{c}{f}$, where $c = 1\,500\,\mathrm{m\,s^{-1}}$ is the acoustic speed in water and f, is the given frequency of vibration. It is instructive that the radiating surface areas must be the same for all the piston sources to make a realistic comparison of their acoustic beam characteristics. Consequently, the *HSL* of all polygon surfaces are determined at the equivalent surface area of the circular piston and expressed in terms of a_c as shown for the triangle in Equation (1). From this equation, the *HSL* of the triangle a_t is determined as given in Equation (2). Similarly, the *HSL* for the rectangle and the square are derived from the equivalent circular surface area as given in Equations (3) and (4), respectively.

$$\frac{1}{2} \times 2a_t \times a_t \tan 60 = \pi {a_c}^2, \tag{1}$$

$$a_t = \left(\sqrt{\pi \tan \frac{\pi}{6}}\right) a_c = \left(\sqrt[4]{\frac{\pi^2}{3}}\right) a_c, \tag{2}$$

$$a_r = \frac{\pi}{4} a_c, \tag{3}$$

$$a_s = \frac{\sqrt{\pi}}{2} a_c. \tag{4}$$

For the high-sided polygons such as the pentagon shown in Figure 3, the equivalent area is expressed in Equation (5) and the *HSL*, a_p is determined as given in Equation (6). Following the same approach for other polygons, it can be found that the *HSL* takes the general form of Equation (7), which is true for all the polygons where n is the number of sides except the rectangle, which is non-regular.

$$5 \times \frac{1}{2} \times 2a_p \times a_p \tan 54 = \pi {a_c}^2, \tag{5}$$

$$a_p = \left(\sqrt{\frac{\pi}{5} \tan \frac{\pi}{5}}\right) a_c. \tag{6}$$

Then, generally for all the n-sided regular polygons, the *HSL* is:

$$\therefore \left(\sqrt{\frac{\pi}{n} \tan \frac{\pi}{n}}\right) a_c. \tag{7}$$

3. Derivation of the directional factors of the acoustic piston surfaces

This section describes the procedures for the derivation of the beam patterns for all the sources with the assumption that all the pistons are mounted on rigid baffles.

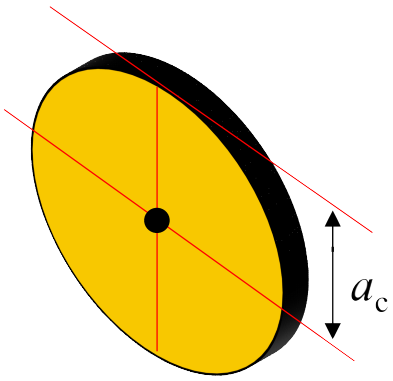

FIGURE 1. The reference circular piston.

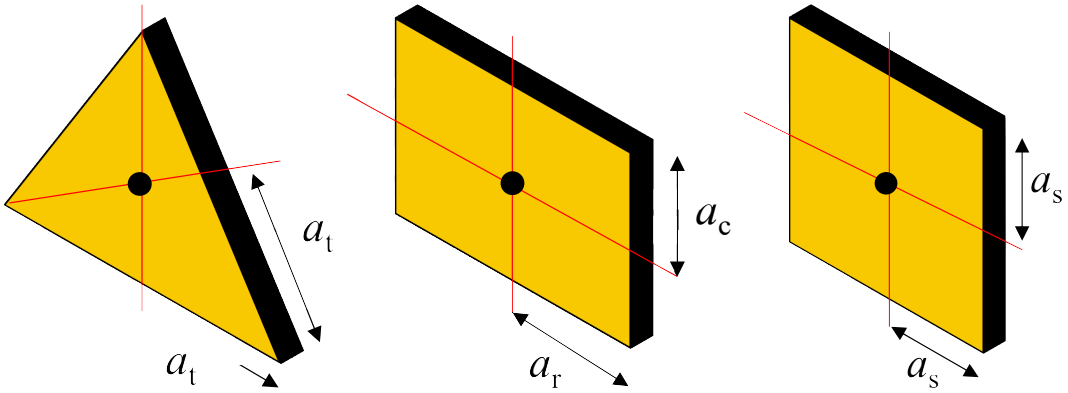

(A). Triangle. (B). Rectangle. (C). Square.

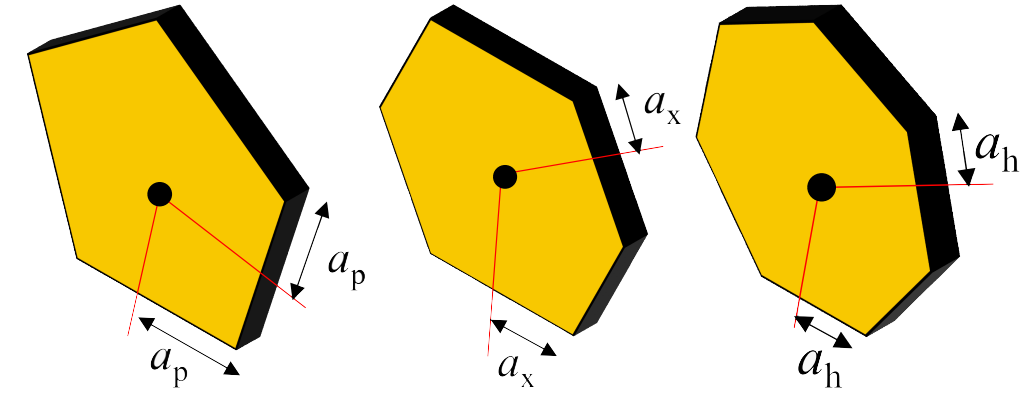

(D). Pentagon. (E). Hexagon. (F). Heptagon.

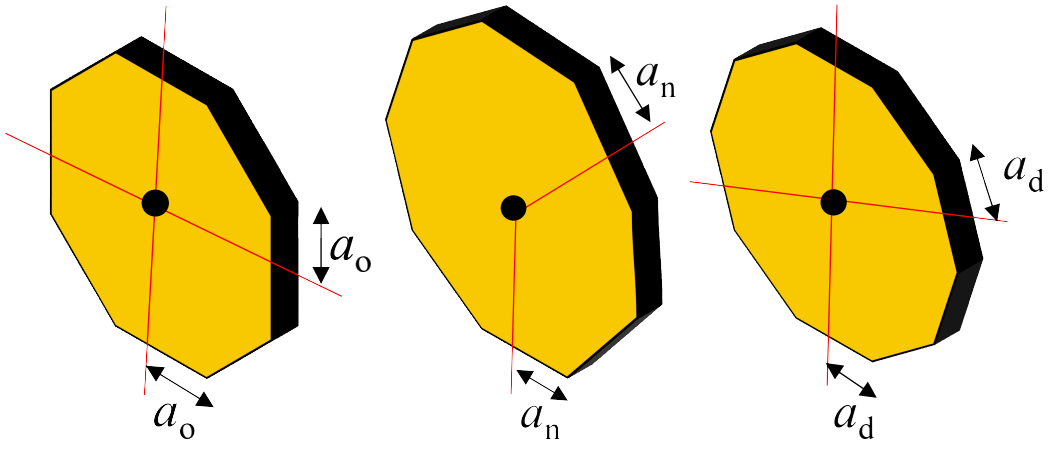

(G). Octagon. (H). Nonagon. (I). Decagon.

FIGURE 2. The polygonal piston surfaces.

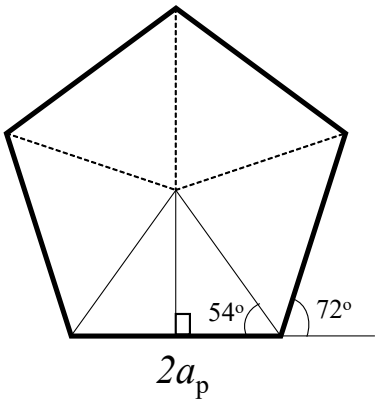

FIGURE 3. The pentagon surface area geometry.

3.1. CIRCULAR PISTON

The directional factor of a circular piston on a rigid baffle is well known [24]. However, it would be derived again in this study to set a general background for the approach to be used for the polygons. Consider an acoustic element of a *HSL*, AB and a small thickness dx whose centre A is located at distance x from the centre C of the circular piston as shown in Figure 4. The piston is considered to be on a rigid baffle such that acoustic radiation is projected in the forward direction from its surface into a point Q at an angle θ from the vertical acoustic axis. Point Q is located at distances R and r from the centres C and A, respectively. Taking AP as a wave front perpendicular to CQ, the relationship between CP and x can be found as expressed in Equation (8). Considering that R and r are distances in the far-field, the line CQ and AQ are parallel resulting into Equation (9).

$$CP = x \sin\theta, \tag{8}$$

$$r = R - CP = R - x \sin\theta. \tag{9}$$

The total acoustic pressure radiated from the acoustic element, p_c can be calculated using the Rayleigh integral over the entire region of the piston surface as expressed in Equation (10). In this equation, $\boldsymbol{A}$ is a constant which depends on certain properties of the medium, namely the wave and the acoustic element. ω is the angular frequency, k is the wave constant and t is the time of wave propagation. dS is the cross-sectional surface area of the element calculated as the product of the total length and thickness dx, i.e. $2(AB)dx$. Determining AB from Figure 4, dS can be expressed as shown in Equation (11).

$$p_c = i \int_{-a_c}^{a_c} \frac{\boldsymbol{A}}{r} e^{i(\omega t - kr)} dS, \tag{10}$$

$$dS = 2 \times AB \times dx = 2\sqrt{{a_c}^2 - x^2}\, dx. \tag{11}$$

Substituting Equations (9) and (11) in Equation (10) while applying the condition that point Q is at the far-field distance, i.e. $\frac{1}{r} \approx \frac{1}{R}$, the constant amplitude is taken out and p_c takes the form of Equation (12). Considering only the real part of the exponents under the integral to preserve the pressure as a complex component of the whole expression, Equation (13) is obtained. If x is set to $a_c \cos\theta$ the integral is transformed into Equation (14), which is simplified where J_1 is a Bessel's function of the first kind as shown in [25]. The directional factor H_c is the absolute value of the angular component isolated as expressed in Equation (15). Using the same approach, directional factors of other surfaces would be derived accordingly in their respective sections. The major difference in the analytical procedure is the determination of the *HSL*, AB for each surface.

$$p_c = i\frac{\boldsymbol{A}}{R} 2e^{i(\omega t - kR)} \int_{-a_c}^{a_c} e^{ikx\sin\theta} \sqrt{{a_c}^2 - x^2}\, dx, \tag{12}$$

$$p_c = i\frac{\boldsymbol{A}}{R} 2e^{i(\omega t - kR)} \int_{-a_c}^{a_c} \cos(kx\sin\theta) \sqrt{{a_c}^2 - x^2}\, dx, \tag{13}$$

$$\begin{aligned} p_c &= i\frac{\boldsymbol{A}}{R} 2{a_c}^2 e^{i(\omega t - kR)} \int_0^{\pi} \cos(ka_c \cos\theta \sin\theta) \sin^2\theta\, d\theta \\ &= i\frac{\boldsymbol{A}}{R} 2\pi {a_c}^2 e^{i(\omega t - kR)} \frac{J_1(ka_c \sin\theta)}{ka_c \sin\theta}, \end{aligned} \tag{14}$$

$$H_c(\theta) = \left| \frac{2J_1(ka_c \sin\theta)}{ka_c \sin\theta} \right|. \tag{15}$$

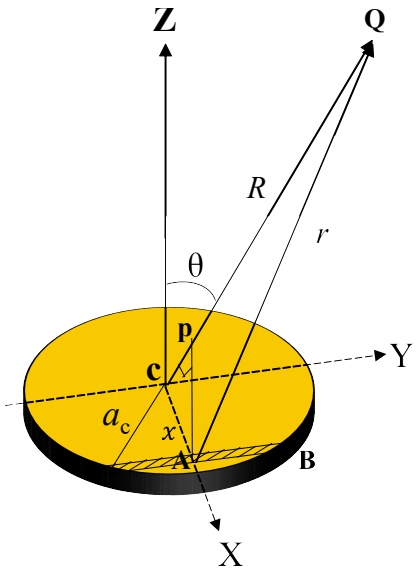

FIGURE 4. The surface geometry for the derivation of the directional factor of a circular piston.

3.2. TRIANGULAR PISTON

For the triangle piston, the centre C is located from the base and top of the surface as shown in Figure 5. The point C is not located at the exact mid-point, hence the surface is non-symmetry. The total pressure integral for the triangular piston takes the form of Equation (16). The AB of the acoustic element on the surface is determined using the principle of similar triangles as given in Equation (17). Substituting r as previously defined in Equation (9) and $dS = 2(AB)dx$ while retaining only the real component of the exponential as previously done in the case of the circular piston in Section 3.1, Equation (16) becomes Equation (18). Then, the complex component of the pressure, p_t is simplified as can be seen from Equations (19)–(21). On further manipulation in Equation (22), p_t takes the final form expressed in Equation (23) from which the directional factor is isolated as Equation (24).

$$P_t = i\int_{-\frac{1}{\sqrt{3}}a_t}^{\frac{2}{\sqrt{3}}a_t} \frac{\boldsymbol{A}}{r} e^{i(\omega t - kr)} dS, \tag{16}$$

$$\frac{CE}{CE+x} = \frac{CD}{AB} = \frac{CE\tan 30}{AB} \therefore AB = \frac{2}{3}a_t + \frac{1}{\sqrt{3}}x, \tag{17}$$

$$p_t = i\frac{\boldsymbol{A}}{r} e^{i(\omega t - kR)} \int_{-\frac{1}{\sqrt{3}}a_t}^{\frac{2}{\sqrt{3}}a_t} \cdot \cos(kx\sin\theta) \cdot 2\left(\frac{2}{3}a_t + \frac{1}{\sqrt{3}}x\right) dx, \tag{18}$$

$$\begin{aligned} &= i\frac{\boldsymbol{A}}{R} 2e^{i(\omega t - kR)} \left\{ \frac{2}{3}a_t \left(\left| \frac{\sin(kx\sin\theta)}{k\sin\theta} \right|_{-\frac{1}{\sqrt{3}}a_t}^{\frac{2}{\sqrt{3}}a_t} \right) \right. \\ &\left. + \frac{1}{\sqrt{3}} \left(\left| \frac{x\sin(kx\sin\theta)}{k\sin\theta} \right|_{-\frac{1}{\sqrt{3}}a_t}^{\frac{2}{\sqrt{3}}a_t} \right) + \frac{1}{\sqrt{3}} \left(\left| \frac{\cos(kx\sin\theta)}{k^2\sin^2\theta} \right|_{-\frac{1}{\sqrt{3}}a_t}^{\frac{2}{\sqrt{3}}a_t} \right) \right\}, \end{aligned} \tag{19}$$

$$\begin{aligned} &= i\frac{\boldsymbol{A}}{R} 2e^{i(\omega t - kR)} \left[\frac{2}{3}a_t \left\{ \frac{\sin\left(k\frac{2}{\sqrt{3}}a_t\sin\theta\right) + \sin\left(k\frac{1}{\sqrt{3}}a_t\sin\theta\right)}{k\sin\theta} \right\} \right. \\ &\left. + \left\{ \frac{\frac{2}{3}a_t\sin\left(k\frac{2}{\sqrt{3}}a_t\sin\theta\right) - \frac{1}{3}a_t\sin\left(k\frac{1}{\sqrt{3}}a_t\sin\theta\right)}{k\sin\theta} \right\} + \frac{1}{\sqrt{3}} \left\{ \frac{\cos\left(k\frac{2}{\sqrt{3}}a_t\sin\theta\right) - \cos\left(k\frac{1}{\sqrt{3}}a_t\sin\theta\right)}{k^2\sin^2\theta} \right\} \right], \end{aligned} \tag{20}$$

$$\begin{aligned} p_t = i\frac{\boldsymbol{A}}{R} 2e^{i(\omega t - kR)} &\left[\frac{4}{3}a_t \left\{ \frac{\sin\left(k\frac{2}{\sqrt{3}}a_t\sin\theta\right)}{k\sin\theta} \right\} + \frac{1}{3}a_t \left\{ \frac{\sin\left(k\frac{1}{\sqrt{3}}a_t\sin\theta\right)}{k\sin\theta} \right\} \right. \\ &\left. - \frac{2}{\sqrt{3}} \left\{ \frac{\sin\left(k\frac{\sqrt{3}}{2}a_t\sin\theta\right)\sin\left(k\frac{\sqrt{3}}{6}a_t\sin\theta\right)}{k^2\sin^2\theta} \right\} \right], \end{aligned} \tag{21}$$

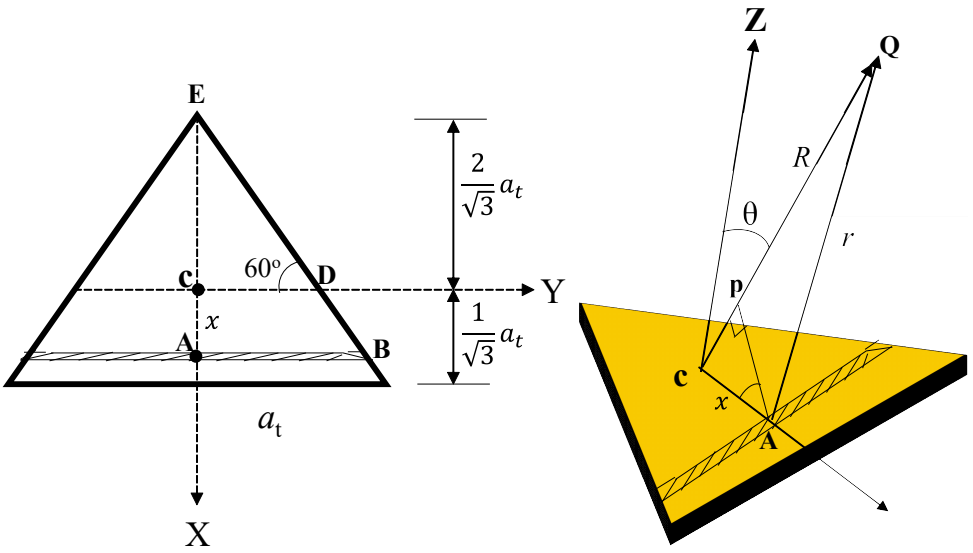

(A). Surface analysis. (B). Radiation analysis.

FIGURE 5. The geometry for the derivation of the directional factor of a triangular acoustic piston source.

$$= i\frac{\boldsymbol{A}}{R}2e^{i(\omega t-kR)}\left[\frac{8}{3\sqrt{3}}{a_t}^2\left\{\frac{\sin\left(k\frac{2}{\sqrt{3}}a_t\sin\theta\right)}{k\frac{2}{\sqrt{3}}a_t\sin\theta}\right\}+\frac{1}{3\sqrt{3}}{a_t}^2\left\{\frac{\sin\left(k\frac{1}{\sqrt{3}}a_t\sin\theta\right)}{k\frac{1}{\sqrt{3}}a_t\sin\theta}\right\}\right.$$
$$\left.-\frac{1}{2\sqrt{3}}{a_t}^2\left\{\frac{\sin\left(k\frac{\sqrt{3}}{2}a_t\sin\theta\right)}{k\frac{\sqrt{3}}{2}a_t\sin\theta}\cdot\frac{\sin\left(k\frac{\sqrt{3}}{6}a_t\sin\theta\right)}{k\frac{\sqrt{3}}{6}a_t\sin\theta}\right\}\right], \tag{22}$$

$$p_t = i\frac{\boldsymbol{A}}{R}\frac{16}{3\sqrt{3}}{a_t}^2e^{i(\omega t-kR)}\left[\frac{\sin\left(k\frac{2}{\sqrt{3}}a_t\sin\theta\right)}{k\frac{2}{\sqrt{3}}a_t\sin\theta}+\frac{1}{8}\left\{\frac{\sin\left(k\frac{1}{\sqrt{3}}a_t\sin\theta\right)}{k\frac{1}{\sqrt{3}}a_t\sin\theta}\right\}\right.$$
$$\left.-\frac{3}{16}\left\{\frac{\sin\left(k\frac{\sqrt{3}}{2}a_t\sin\theta\right)}{k\frac{\sqrt{3}}{2}a_t\sin\theta}\cdot\frac{\sin\left(k\frac{\sqrt{3}}{6}a_t\sin\theta\right)}{k\frac{\sqrt{3}}{6}a_t\sin\theta}\right\}\right], \tag{23}$$

$$H_t = \left|\frac{\sin\left(k\frac{2}{\sqrt{3}}a_t\sin\theta\right)}{k\frac{2}{\sqrt{3}}a_t\sin\theta}+\frac{1}{8}\left\{\frac{\sin\left(k\frac{1}{\sqrt{3}}a_t\sin\theta\right)}{k\frac{1}{\sqrt{3}}a_t\sin\theta}\right\}-\frac{3}{16}\left\{\frac{\sin\left(k\frac{\sqrt{3}}{2}a_t\sin\theta\right)}{k\frac{\sqrt{3}}{2}a_t\sin\theta}\cdot\frac{\sin\left(k\frac{\sqrt{3}}{6}a_t\sin\theta\right)}{k\frac{\sqrt{3}}{6}a_t\sin\theta}\right\}\right|. \tag{24}$$

3.3. RECTANGULAR AND SQUARE PISTONS

The rectangle and the square have identical geometries except that the latter is regular by having equal sides. Consequently, the directional factor when successfully derived for one can be used to predict the other without the repetition of the procedures. The acoustic element lying parallel to the Y-axis on the surface of the rectangular surface is shown in Figure 6. The surface is symmetrical since the centre C is located at the exact midpoint. Since $AB = a_c$ and $dS = 2\,a_c\,dx$, the complex pressure component p_r can then be expressed as Equation (25). This equation is simplified from Equations (26)–(29) and the directional factor of the rectangular surface H_r is then isolated as given in Equation (30). Therefore, the directional factor of the square piston H_s takes the form of Equation (31).

$$p_r = i\frac{\boldsymbol{A}}{r}e^{i(\omega t-kr)}\int_{-a_r}^{a_r}\cos\left(kx\sin\theta\right)2a_c dx, \tag{25}$$

$$= i\frac{\boldsymbol{A}}{r}e^{i(\omega t-kr)}2a_c\left|\frac{\sin\left(kx\sin\theta\right)}{k\sin\theta}\right|_{-a_r}^{a_r}, \tag{26}$$

$$= i\frac{\boldsymbol{A}}{r}e^{i(\omega t-kr)}2a_c\left(\frac{\sin\left(ka_r\sin\theta\right)+\sin\left(ka_r\sin\theta\right)}{k\sin\theta}\right), \tag{27}$$

$$= i\frac{\boldsymbol{A}}{r}e^{i(\omega t-kr)}4a_c\frac{\sin\left(ka_r\sin\theta\right)}{k\sin\theta}, \tag{28}$$

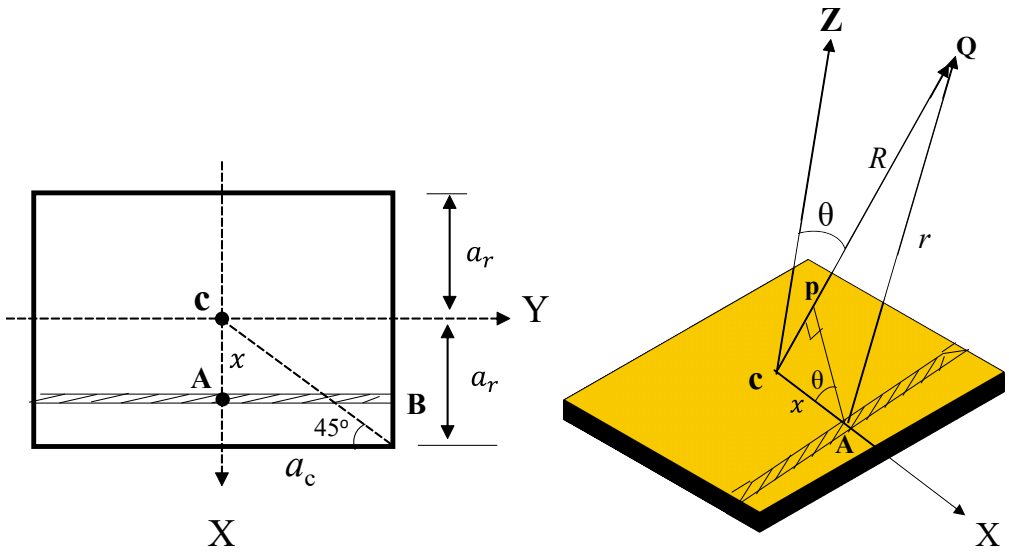

(A). Surface analysis. (B). Radiation analysis.

FIGURE 6. The geometry for the derivation of the directional factor of a rectangular acoustic piston source.

$$p_r = i\frac{\boldsymbol{A}}{r}e^{i(\omega t-kr)}4a_c a_r \frac{\sin(ka_r\sin\theta)}{ka_r\sin\theta}, \tag{29}$$

$$H_r = \left|\frac{\sin(ka_r\sin\theta)}{ka_r\sin\theta}\right| = \left|\frac{\sin(ka_r\tan 45\sin\theta)}{ka_r\tan 45\sin\theta}\right|, \tag{30}$$

$$H_s = \left|\frac{\sin(ka_s\sin\theta)}{ka_s\sin\theta}\right| = \left|\frac{\sin(ka_s\tan 45\sin\theta)}{ka_s\tan 45\sin\theta}\right|. \tag{31}$$

3.4. PENTAGONAL PISTON

Figure 7 shows the location of the centre C with respect to the top and bottom of the radiation surface of a regular pentagon. Just like the triangle, the surface is non-symmetrical since the point C is not located at the exact midpoint of the surface. The height of the extruded triangle as given in the figure allows us to find the *HSL*, AB of the acoustic element on that surface by the principle of similar triangles as given in Equation (32). Consequently, the integral for calculating the complex component of the pressure p_p is given in Equation (33) and simplified through Equations (34)–(36). When further manipulated mathematically, Equation (36) can be expressed as given in Equation (37). From this equation, the directional factor for the pentagon surface H_p can be isolated as given in Equation (38), Applying trigonometry identity, this equation is further worked down through Equations (39)–(40).

$$\frac{a_p\tan 72}{a_p\tan 72+(a_p\tan 54-x)} = \frac{a_p}{AB} \therefore AB = (1+\tan 54\tan 18)\,a_p - x\tan 18, \tag{32}$$

$$P_p = i\frac{\boldsymbol{A}}{r}e^{i(\omega t-kR)}\int_{-a_p\tan 54}^{\frac{1}{\cos 54}a_p}\cos(kx\sin\theta)\cdot\{(1+\tan 54\tan 18)\,a_p - x\tan 18\}\,dx \tag{33}$$

$$\begin{aligned}&= i\frac{\boldsymbol{A}}{R}2e^{i(\omega t-kR)}\left\{(1+\tan 54\tan 18)\,a_p\left(\left|\frac{\sin(kx\sin\theta)}{k\sin\theta}\right|\begin{matrix}a_p\sec 54\\-a_p\tan 54\end{matrix}\right)\right.\\&\quad\left.-\tan 18\left(\left|\frac{x\sin(kx\sin\theta)}{k\sin\theta}\right|\begin{matrix}a_p\sec 54\\-a_p\tan 54\end{matrix}\right)-\tan 18\left(\left|\frac{\cos(kx\sin\theta)}{k^2\sin^2\theta}\right|\begin{matrix}a_p\sec 54\\-a_p\tan 54\end{matrix}\right)\right\}\end{aligned} \tag{34}$$

$$\begin{aligned}&= i\frac{\boldsymbol{A}}{R}2e^{i(\omega t-kR)}\left[(1+\tan 54\tan 18)\,a_p\left\{\frac{\sin(ka_p\sec 54\sin\theta)+\sin(ka_p\tan 54\sin\theta)}{k\sin\theta}\right\}\right.\\&\quad-\left\{\frac{(\tan 18\sec 54)\,a_p\sin(ka_p\sec 54\sin\theta)-(\tan 18\tan 54)\,a_p\sin(ka_p\tan 54\sin\theta)}{k\sin\theta}\right\}\\&\quad\left.-\tan 18\left\{\frac{\cos(ka_p\sec 54\sin\theta)-\cos(ka_p\tan 54\sin\theta)}{k^2\sin^2\theta}\right\}\right]\end{aligned} \tag{35}$$

$$= i\frac{\boldsymbol{A}}{R}2e^{i(\omega t-kR)}\left[(1+\tan 54\tan 18-\tan 18\sec 54)\,a_p\left\{\frac{\sin\left(ka_p\sec 54\sin\theta\right)}{k\sin\theta}\right\}\right.$$
$$+(1+2\tan 54\tan 18)\,a_p\left\{\frac{\sin\left(ka_p\tan 54\sin\theta\right)}{k\sin\theta}\right\} \tag{36}$$
$$\left.+\frac{2\tan 18}{k^2\sin^2\theta}\left[\sin\left\{k\left(\frac{\sec 54+\tan 54}{2}\right)a_p\sin\theta\right\}\sin\left\{k\left(\frac{\sec 54-\tan 54}{2}\right)a_{\ p}\sin\theta\right\}\right]\right],$$

$$P_p = i\frac{\boldsymbol{A}}{R}2{a_p}^2e^{i(\omega t-kR)}\left[\sec 54\left\{1+\tan 18\left(\tan 54-\sec 54\right)\right\}\left\{\frac{\sin\left(ka_p\sec 54\sin\theta\right)}{ka_p\sec 54\sin\theta}\right\}\right.$$
$$+\tan 54\left(1+2\tan 54\tan 18\right)\left\{\frac{\sin\left(ka_p\tan 54\sin\theta\right)}{ka_p\tan 54\sin\theta}\right\} \tag{37}$$
$$\left.+\frac{\tan 18}{2}\left[\frac{\sin\left\{k\left(\frac{\sec 54+\tan 54}{2}\right)a_{\ p}\sin\theta\right\}}{k\left(\frac{\sec 54+\tan 54}{2}\right)a_{\ p}\sin\theta}\cdot\frac{\sin\left\{k\left(\frac{\sec 54-\tan 54}{2}\right)a_{\ p}\sin\theta\right\}}{k\left(\frac{\sec 54-\tan 54}{2}\right)a_{\ p}\sin\theta}\right]\right],$$

$$H_p = \left|\sec 54\left\{1+\tan 18\left(\tan 54-\sec 54\right)\right\}\left\{\frac{\sin\left(ka_p\sec 54\sin\theta\right)}{ka_p\sec 54\sin\theta}\right\}\right.$$
$$+\tan 54\left(1+2\tan 54\tan 18\right)\left\{\frac{\sin\left(ka_p\tan 54\sin\theta\right)}{ka_p\tan 54\sin\theta}\right\} \tag{38}$$
$$\left.+\frac{\tan 18}{2}\left[\frac{\sin\left\{k\left(\frac{\sec 54+\tan 54}{2}\right)a_{\ p}\sin\theta\right\}}{k\left(\frac{\sec 54+\tan 54}{2}\right)a_{\ p}\sin\theta}\cdot\frac{\sin\left\{k\left(\frac{\sec 54-\tan 54}{2}\right)a_{\ p}\sin\theta\right\}}{k\left(\frac{\sec 54-\tan 54}{2}\right)a_{\ p}\sin\theta}\right]\right|$$
$$= \left|\sec 54\left\{1+\left(\frac{\sec 54-\tan 54}{\tan 108}\right)\right\}\left\{\frac{\sin\left(ka_p\sec 54\sin\theta\right)}{ka_p\sec 54\sin\theta}\right\}\right.$$
$$+\tan 54\left(1-\frac{2\tan 54}{\tan 108}\right)\left\{\frac{\sin\left(ka_p\tan 54\sin\theta\right)}{ka_p\tan 54\sin\theta}\right\} \tag{39}$$
$$\left.-\frac{1}{2\tan 108}\left[\frac{\sin\left\{k\left(\frac{\sec 54+\tan 54}{2}\right)a_{\ p}\sin\theta\right\}}{k\left(\frac{\sec 54+\tan 54}{2}\right)a_{\ p}\sin\theta}\cdot\frac{\sin\left\{k\left(\frac{\sec 54-\tan 54}{2}\right)a_{\ p}\sin\theta\right\}}{k\left(\frac{\sec 54-\tan 54}{2}\right)a_{\ p}\sin\theta}\right]\right|,$$

$$H_p = \left|\sec 54\left\{1+\left(\frac{\sec 54-\tan 54}{\tan 108}\right)\right\}\left\{\frac{\sin\left(ka_p\sec 54\sin\theta\right)}{ka_p\sec 54\sin\theta}\right\}\right.$$
$$+\tan^3 54\left\{\frac{\sin\left(ka_p\tan 54\sin\theta\right)}{ka_p\tan 54\sin\theta}\right\} \tag{40}$$
$$\left.-\frac{1}{2\tan 108}\left[\frac{\sin\left\{k\left(\frac{\sec 54+\tan 54}{2}\right)a_{\ p}\sin\theta\right\}}{k\left(\frac{\sec 54+\tan 54}{2}\right)a_{\ p}\sin\theta}\cdot\frac{\sin\left\{k\left(\frac{\sec 54-\tan 54}{2}\right)a_{\ p}\sin\theta\right\}}{k\left(\frac{\sec 54-\tan 54}{2}\right)a_{\ p}\sin\theta}\right]\right|.$$

3.5. Hexagonal piston

The position of the centre C of a regular hexagon surface geometry, which is clearly symmetrical, is shown in Figure 8. The *HSL*, AB of the acoustic element on the surface can be found using the similar triangles approach as shown in Equation (41). The complex component of the pressure integral p_x is then given in Equation (42) and evaluated in Equation (43). On further simplification, the middle and the last terms in this equation vanishes and the final expression for the acoustic pressure then becomes Equation (44). Then, the directional factor is isolated as Equation (45).

$$\frac{\sqrt{3}a_x}{a_x} = \frac{AX}{AB} = \frac{\sqrt{3}a_x+\sqrt{3}a_x-x}{AB} \therefore AB = 2a_x-\frac{1}{\sqrt{3}}x, \tag{41}$$

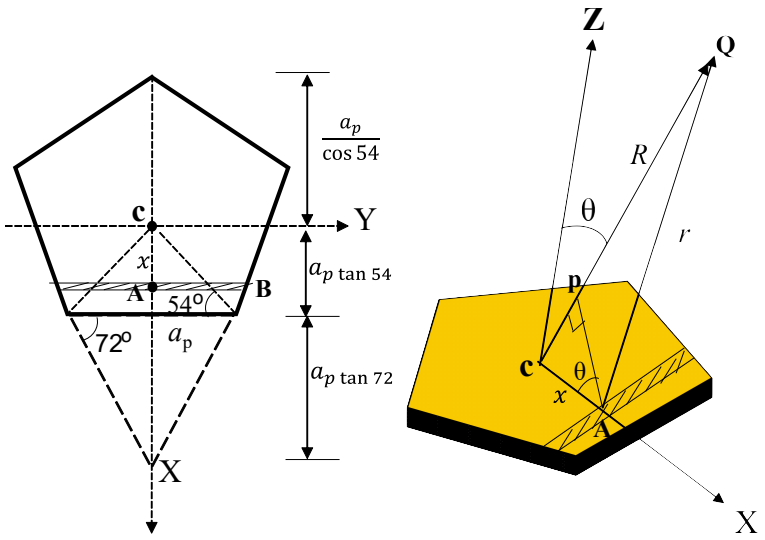

(A). Surface analysis. (B). Radiation analysis.

FIGURE 7. The geometry for the derivation of the directional factor of a pentagonal acoustic piston source.

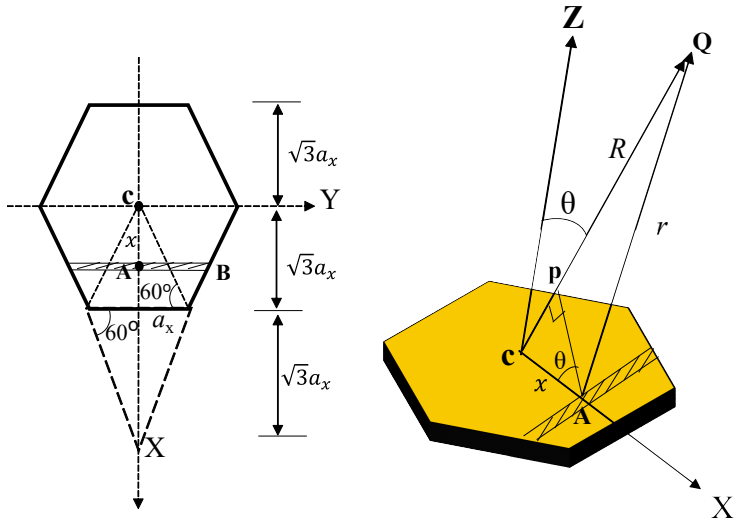

(A). Surface analysis. (B). Radiation analysis.

FIGURE 8. The geometry for the derivation of the directional factor of hexagonal acoustic piston source.

$$P_x = i\frac{\boldsymbol{A}}{R}e^{i(\omega t-kR)}\int_{-\sqrt{3}a_x}^{\sqrt{3}a_x}\cos(kx\sin\theta)\cdot\left(2a_x-\frac{1}{\sqrt{3}}x\right)dx \tag{42}$$

$$\begin{aligned}= i\frac{\boldsymbol{A}}{R}2e^{i(\omega t-kR)}\Bigg\{&2a_x\left(\left|\frac{\sin(kx\sin\theta)}{k\sin\theta}\right|_{-\sqrt{3}a_x}^{\sqrt{3}a_x}\right)\\&-\frac{1}{\sqrt{3}}\left(\left|\frac{x\sin(kx\sin\theta)}{k\sin\theta}\right|_{-\sqrt{3}a_x}^{\sqrt{3}a_x}\right)-\frac{1}{\sqrt{3}}\left(\left|\frac{\cos(kx\sin\theta)}{k^2\sin^2\theta}\right|_{-\sqrt{3}a_x}^{\sqrt{3}a_x}\right)\Bigg\},\end{aligned} \tag{43}$$

$$P_x = i\frac{\boldsymbol{A}}{R}e^{i(\omega t-kR)}8a_x\left(\frac{\sin\left(k\sqrt{3}a_x\sin\theta\right)}{k\sin\theta}\right) = i\frac{\boldsymbol{A}}{R}e^{i(\omega t-kR)}8\sqrt{3}{a_x}^2\frac{\sin\left(k\sqrt{3}a_x\sin\theta\right)}{k\sqrt{3}a_x\sin\theta}, \tag{44}$$

$$H_x = \left|\frac{\sin\left(k\sqrt{3}a_x\sin\theta\right)}{k\sqrt{3}a_x\sin\theta}\right| = \left|\frac{\sin\left(ka_x\tan 60\sin\theta\right)}{ka_x\tan 60\sin\theta}\right|. \tag{45}$$

3.6. Heptagonal piston

The centre C of the regular heptagon with respect to the top and bottom of the non-symmetrical surface is as shown in Figure 9. By the similar triangle principle, the HSL, AB can be determined as given in Equation (46)

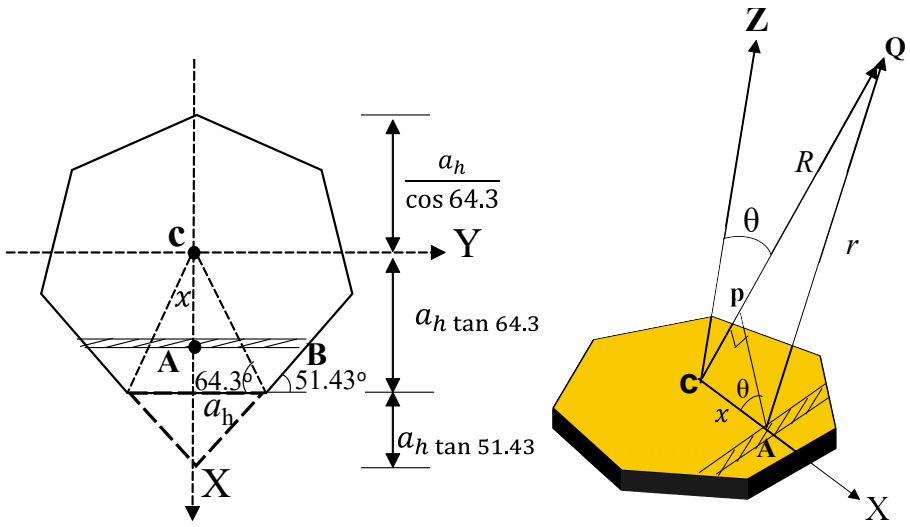

(A). Surface analysis. (B). Radiation analysis.

FIGURE 9. The geometry for the derivation of the directional factor of heptagonal acoustic piston source.

and the complex part of the pressure integral can, therefore, be expressed as in Equation (47). As can be clearly observed from these equations, the heptagon indicates almost an identical geometry with the pentagon analysed in Section 3.4. Thus, without any repetition of the procedure, it is easy to determine that Equation (47) takes the final form of Equation (48). Consequently, the directional factor follows a similar pattern as previously done in Section 3.4, and therefore expressed as Equation (49).

$$\frac{a_h \tan 51.43}{a_h} = \frac{a_h \tan 51.43 + (a_h \tan 64.3 - x)}{AB} \therefore AB = (1 + \tan 64.3 \tan 38.57)\, a_h - x \tan 38.57, \tag{46}$$

$$P_h = i\frac{\boldsymbol{A}}{r} e^{i(\omega t - kR)} \int_{-a_h \tan 64.3}^{\frac{1}{\cos 64.3} a_h} \cos(kx \sin\theta) \cdot 2\left\{(1 + \tan 64.3 \tan 38.57)\, a_h - x \tan 38.57\right\} dx, \tag{47}$$

$$\begin{aligned} P_h = i\frac{\boldsymbol{A}}{R} 2{a_h}^2 e^{i(\omega t - kR)} \Bigg[& \sec 64.3 \left\{1 + \tan 38.57 \left(\tan 64.3 - \sec 64.3\right)\right\} \left\{\frac{\sin(ka_h \sec 64.3 \sin\theta)}{ka_h \sec 64.3 \sin\theta}\right\} \\ & + \tan 64.3 \left(1 + 2 \tan 64.3 \tan 38.57\right) \left\{\frac{\sin(ka_h \tan 64.3 \sin\theta)}{ka_h \tan 64.3 \sin\theta}\right\} \\ & + \frac{\tan 38.57}{2} \left[\frac{\sin\left\{k\left(\frac{\sec 64.3 + \tan 64.3}{2}\right) a_h \sin\theta\right\}}{k\left(\frac{\sec 64.3 + \tan 64.3}{2}\right) a_h \sin\theta} \cdot \frac{\sin\left\{k\left(\frac{\sec 64.3 - \tan 64.3}{2}\right) a_h \sin\theta\right\}}{k\left(\frac{\sec 64.3 - \tan 64.3}{2}\right) a_h \sin\theta}\right]\Bigg], \end{aligned} \tag{48}$$

$$\begin{aligned} H_h = \Bigg| & \sec 64.3 \left\{1 + \left(\frac{\sec 64.3 - \tan 64.3}{\tan 128.6}\right)\right\} \left\{\frac{\sin(ka_h \sec 64.3 \sin\theta)}{ka_h \sec 64.3 \sin\theta}\right\} \\ & + \tan^3 64.3 \left\{\frac{\sin(ka_h \tan 64.3 \sin\theta)}{ka_h \tan 64.3 \sin\theta}\right\} \\ & - \frac{1}{2 \tan 128.6} \left[\frac{\sin\left\{k\left(\frac{\sec 64.3 + \tan 64.3}{2}\right) a_h \sin\theta\right\}}{k\left(\frac{\sec 64.3 + \tan 64.3}{2}\right) a_h \sin\theta} \cdot \frac{\sin\left\{k\left(\frac{\sec 64.3 - \tan 64.3}{2}\right) a_h \sin\theta\right\}}{k\left(\frac{\sec 64.3 - \tan 64.3}{2}\right) a_h \sin\theta}\right]\Bigg|. \end{aligned} \tag{49}$$

3.7. OCTAGONAL PISTON

Figure 10 shows the centre C of the regular octagon piston surface with a nearly identical symmetrical geometry to the hexagon. Following the same analytical procedures as previously undertaken in Section 3.5, the *HSL*, *AB*, the complex pressure component, p_o, and the directional factor are derived as expressed in Equations (50)–(52), respectively.

$$\frac{a_0}{a_0} = \frac{a_0 + a_0\left(1 + \sqrt{2}\right) - x}{AB} \therefore AB = \left(2 + \sqrt{2}\right) a_o - x, \tag{50}$$

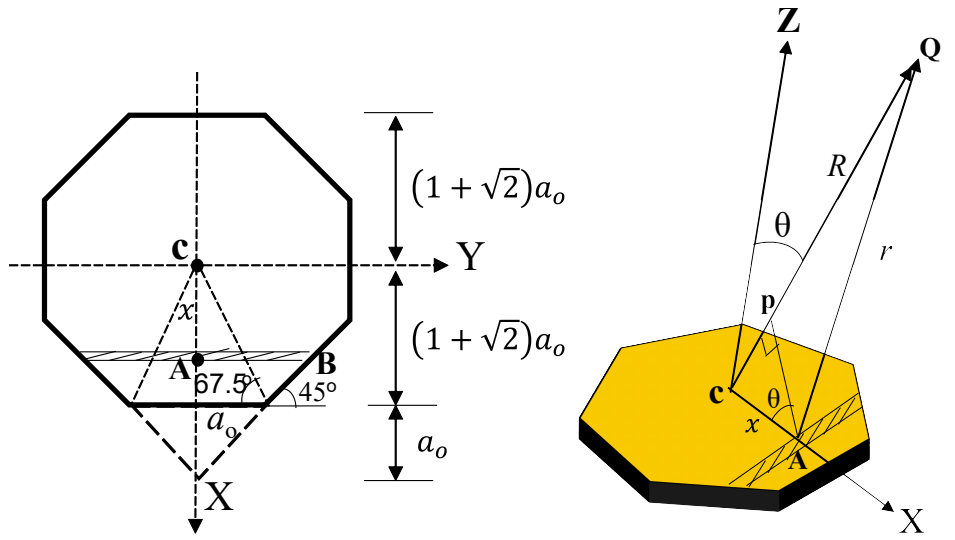

(A). Surface analysis. (B). Radiation analysis.

Figure 10. The geometry for the derivation of the directional factor of octagonal piston source.

$$\begin{aligned} p_o &= i\frac{\boldsymbol{A}}{r}e^{i(\omega t-kR)}\int_{-(1+\sqrt{2})a_0}^{(1+\sqrt{2})a_0}\cos\left(kx\sin\theta\right)\cdot 2\left\{\left(2+\sqrt{2}\right)a_o - x\right\}dx \\ &= i\frac{\boldsymbol{A}}{R}e^{i(\omega t-kR)}4{a_o}^2\left(4+3\sqrt{2}\right)\frac{\sin\left(k\left(1+\sqrt{2}\right)a_0\sin\theta\right)}{k\left(1+\sqrt{2}\right)a_0\sin\theta}, \end{aligned} \tag{51}$$

$$H_0 = \left|\frac{\sin\left(k\left(1+\sqrt{2}\right)a_0\sin\theta\right)}{k\left(1+\sqrt{2}\right)a_0\sin\theta}\right| = \left|\frac{\sin\left(ka_0\tan 67.5\sin\theta\right)}{ka_0\tan 67.5\sin\theta}\right|. \tag{52}$$

3.8. Nonagonal piston

Like the heptagon, Figure 11 clearly shows that a non-symmetrical surface geometry of a regular nonagon, which is closely similar to that of the pentagon studied in Section 3.4. Then, AB and the complex pressure component, p_n are given as Equations (53) and (54), respectively. Hence, it is easy to identify that the directional factor is in the form given in Equation (55).

$$AB = (1+\tan 70\tan 50)\,a_n - x\tan 50, \tag{53}$$

$$\begin{aligned} p_n = i\frac{\boldsymbol{A}}{R}2{a_n}^2e^{i(\omega t-kR)}\Bigg[&\sec 70\left\{1+\tan 50\left(\tan 70-\sec 70\right)\right\}\left\{\frac{\sin\left(ka_n\sec 70\sin\theta\right)}{ka_n\sec 70\sin\theta}\right\} \\ &+\tan 70\left(1+2\tan 70\tan 50\right)\left\{\frac{\sin\left(ka_n\tan 70\sin\theta\right)}{ka_n\tan 70\sin\theta}\right\} \\ &+\frac{\tan 50}{2}\left[\frac{\sin\left\{k\frac{(\sec 70+\tan 70)}{2}a_n\sin\theta\right\}}{k\frac{(\sec 70+\tan 70)}{2}a_n\sin\theta}\cdot\frac{\sin\left\{k\frac{(\sec 70-\tan 70)}{2}a_n\sin\theta\right\}}{k\frac{(\sec 70-\tan 70)}{2}a_n\sin\theta}\right]\Bigg], \end{aligned} \tag{54}$$

$$\begin{aligned} H_n = \sec 70&\left\{1+\left(\frac{\sec 70-\tan 70}{\tan 140}\right)\right\}\left\{\frac{\sin\left(ka_n\sec 70\sin\theta\right)}{ka_n\sec 70\sin\theta}\right\}+\tan^3 70\left\{\frac{\sin\left(ka_n\tan 70\sin\theta\right)}{ka_n\tan 70\sin\theta}\right\} \\ &-\frac{1}{2\tan 140}\left[\frac{\sin\left\{k\left(\frac{\sec 70+\tan 70}{2}\right)a_n\sin\theta\right\}}{k\left(\frac{\sec 70+\tan 70}{2}\right)a_n\sin\theta}\cdot\frac{\sin\left\{k\left(\frac{\sec 70-\tan 70}{2}\right)a_n\sin\theta\right\}}{k\left(\frac{\sec 70-\tan 70}{2}\right)a_n\sin\theta}\right]. \end{aligned} \tag{55}$$

3.9. Decagonal piston

Like the octagon in Section 3.7, Figure 12 indicates a clear symmetrical similarity with the hexagon studied in Section 3.5. Consequently, following similar analytical procedures while avoiding repetitions, the directional factor of the octagonal piston can be expressed as:

$$H_d = \left|\frac{\sin\left(ka_d\tan 72\sin\theta\right)}{ka_d\tan 72\sin\theta}\right|. \tag{56}$$

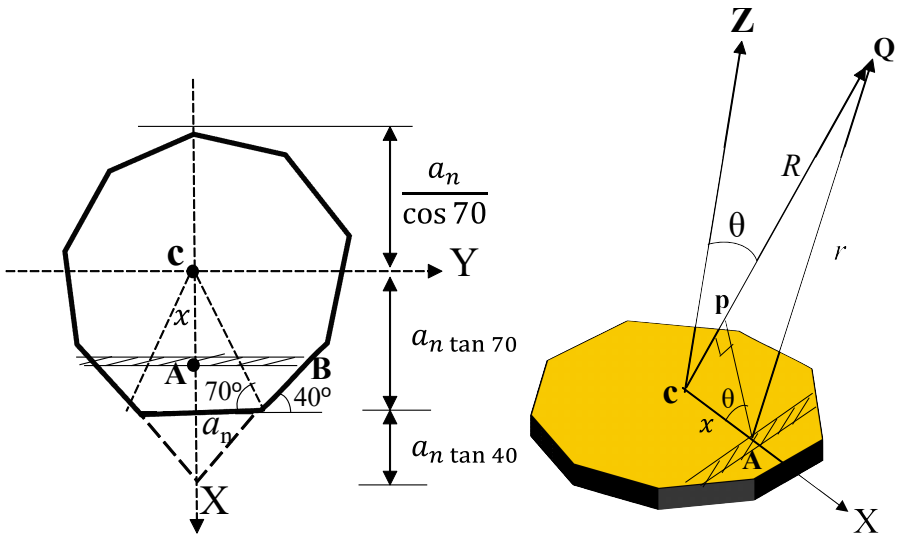

(A). Surface analysis. (B). Radiation analysis.

FIGURE 11. The geometry for the derivation of the directional factor of nonagonal acoustic piston source.

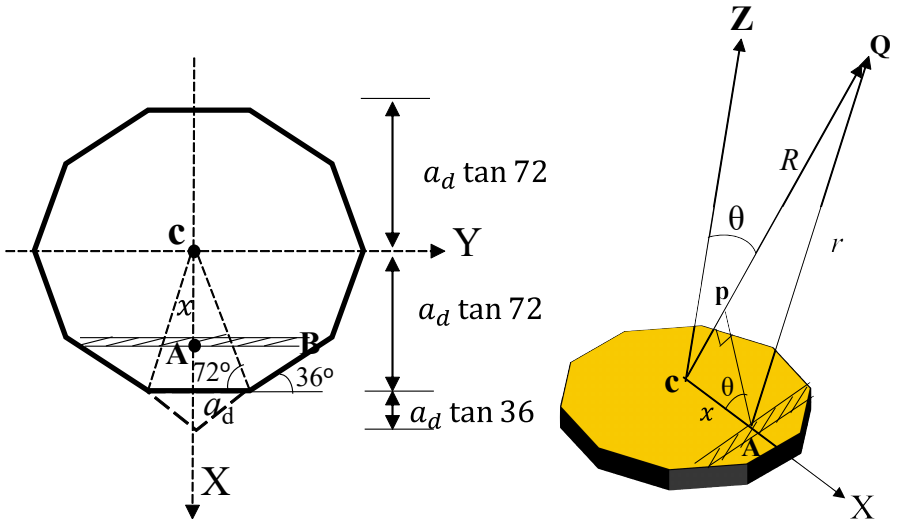

(A). Surface analysis. (B). Radiation analysis.

FIGURE 12. The surface geometry for the derivation of the directional factor of decagonal acoustic piston source.

4. The analysis and characterisation of the beam patterns

For each piston surface, the beam pattern is determined using Equation (57) where H is the directional factor and $H_{\max}$ is its maximum value. The comparative plots of the beam patterns for all the pistons calculated at different diameters of the standard circular surface using the respective directional factors derived in Section 3 is shown in Figure 13. The circular diameters range from 0.28–3.0λ since the directivity of a circular transducer is high enough when the diameter is greater than 2λ [26]. The quantitative comparison of the results indicating the half-power (−3 dB) beam width (BW) of the main lobe as well as the side lobe level (SLL) of the beam patterns is presented in Table 1.

$$\text{beam pattern} = 20 \log \left| \frac{H}{H_{max}} \right|. \tag{57}$$

These results show that all the pistons of the same surface area exhibit a similar performance with a circular piston having a diameter not greater than 0.28λ or being as large as 0.43λ when the triangle is excluded. Meanwhile, the rectangular and circular pistons of equal surface area still maintain similar radiation patterns as long as the circular diameter is still within a half wavelength. Above this, the odd-sided non-symmetrical polygon surfaces appear to have a relatively lower beam width compared to the symmetrical ones. This finding is contrary to what is reported by [19] who adopted the square as a rectangular piston and reported that octagonal, hexagonal, rectangular, and circular pistons exhibit completely omnidirectional beam patterns when the surface area is equivalent to the circular diameter of 0.5λ.

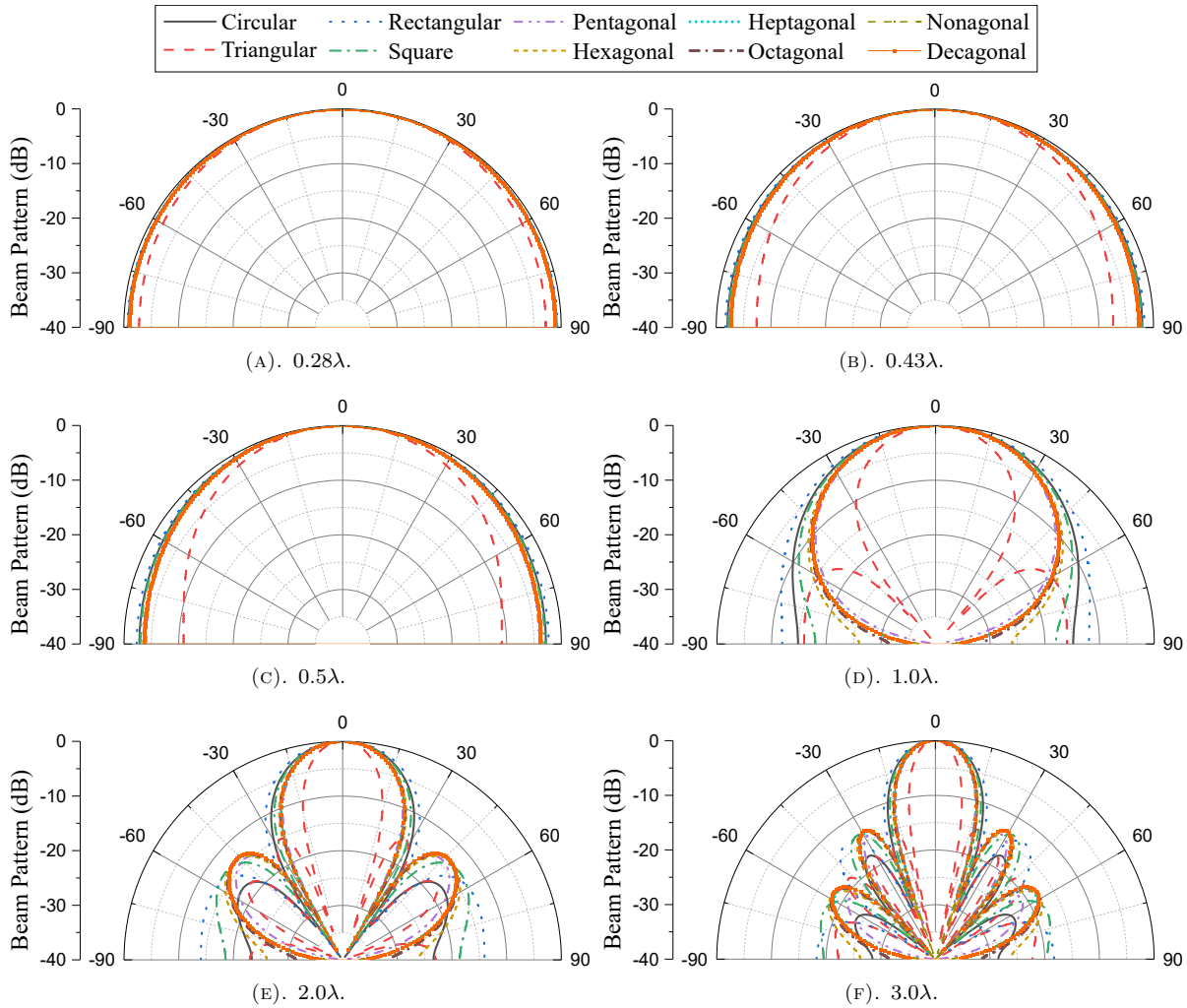

(A). 0.28λ. (B). 0.43λ.

(C). 0.5λ. (D). 1.0λ.

(E). 2.0λ. (F). 3.0λ.

Figure 13. The beam pattern of polygonal piston surfaces of equal surface area with a circular piston of different diameters.

Piston sources	The diameter of the circular piston								
	0.28λ	**0.43λ**	**0.5λ**	**1.0λ**		**2.0λ**		**3.0λ**	
	BW [°]	**BW [°]**	**BW [°]**	**BW [°]**	**SLL [dB]**	**BW [°]**	**SLL [dB]**	**BW [°]**	**SLL [dB]**
Circular	180	180	180	61.9	-	29.8	−17.6	19.8	−17.5
Triangular	180	84.3	70.5	33.6	−15.1	16.7	−15.1	11.1	−15.1
Rectangular	180	180	180	68.6	-	32.7	−13.3	21.7	−13.2
Square	180	180	173.1	59.9	-	28.9	−13.3	19.2	−13.2
Pentagonal	180	180	121.2	51.7	-	25.2	−14.2	16.8	−14.2
Hexagonal	180	180	136.5	55.4	-	26.9	−13.3	17.9	−13.2
Heptagonal	180	180	127.6	53.3	-	26.0	−13.4	17.3	−13.4
Octagonal	180	180	130.6	54.1	-	26.3	−13.3	17.5	−13.2
Nonagonal	180	180	127.5	53.3	-	26.0	−13.3	17.3	−13.3
Decagonal	180	180	128.2	53.5	-	26.1	−13.3	17.3	−13.2

Table 1. The −3 dB beam pattern of the polygonal pistons of the same surface area with a circular piston of different diameters.

Meanwhile, the circular piston is better than all the polygons in terms of its side lobe level. However, it is worse in terms of its beam width compared to the rectangular piston and not much significantly different from the square. Coincidentally, the closeness observed in the radiation beam patterns between the square and circular pistons had equally been reported for their radiation impedances [27]. The side lobe levels remain the same at less than −13 dB for all other polygons but lower than −14 dB for the triangular and pentagonal pistons. Notably, the radiation pattern of the triangular piston is completely unique from other polygon surfaces. It has

a narrower beam width, one side lobe higher than the others, and the lowest side lobe level next to the circular piston. Perhaps, this explains why it does not appear to have any practical application, nor is it well known in the literature [28].

For the number of sides higher than five, the radiation beam characteristics are almost identical for all the polygons. Nevertheless, the hexagonal piston seems to be the best while heptagonal, nonagonal, and decagonal ones are generally the same. One would expect that the performance characteristics of the acoustic polygonal pistons become closer to the circular piston as the number of sides increases. However, this result has shown that neither the surface area nor the number of sides of the polygon influences the radiation pattern. Rather, it is the combination of the perimeter and the symmetry of the surface. At equal surface area, all the polygons are higher in perimeter than the circle while their perimeter decreases as the number of sides increases in order of their list in Table 1. The triangle, which has the highest perimeter, exhibits the narrowest beamwidth due to its non-symmetry while the rectangle and square ones have the first and second overall dominance. Consequently, the surface symmetry factor takes precedence over the perimeter such as in the case of the hexagon and octagon relative to the pentagon and in the case of the last four polygons relative to one another.

5. Validation by finite element method

To prove the correctness of the directional factors of each acoustic polygonal piston source proposed in this study, the finite element method (FEM) was employed for the validation of the radiation patterns using the Pzflex® commercial software. The first eight pistons were selected while the remaining two were left out since their directional factors are essentially the same with the polygons having either the odd or even number of sides and their performance is not dissimilar with the heptagonal piston.

Each of the piston surfaces was modelled as the head masses of a Tonpilz transducer made of aluminium using the FEM as shown for the standard circular source in Figure 14a. The tail mass at the rear end is a brass material serving as a rigid baffle while the piezo-ceramic drive section is sandwiched in-between. The selected piezoelectric ceramic material was KP14 (Kyoungwon Ferrite Co. Ltd). The head mass was designed at the equivalent circular diameter of 1.0λ for all the radiating surfaces corresponding to the equivalent surface area derived for each piston source in the theoretical analysis. Since the transducer vibrates in the longitudinal mode, the thickness of the drive section and all other dimensions were determined by the resonance frequency of operation. For the finite element analysis (FEA), water was modelled at the front of each surface as shown for the standard circular head mass in Figure 14b. The final mesh of the structure was simulated at an element size of $\frac{1}{32}$ factor of the wavelength. The absorption boundary condition was applied all around the water to avoid a loss of acoustic signals being transmitted through the application of a pressure pulse in the form of a sine wave function and 1 volt of electrical energy to drive the ceramics. Figure 15 shows the models of the selected polygon surfaces analysed following similar procedures. The result of the comparison between the theoretical beam patterns and that obtained from the FEA for each of the surfaces are shown in Figure 16. Except with a little difference of about 2 dB in the triangular case, the excellent agreements observed in Figure 16 for all the selected cases is a strong attestation to the validity of the directional factors invented for the radiating polygonal pistons.

6. Summary

The directional factors of acoustic polygonal piston sources with surfaces ranging from three to ten sides have been derived and used to characterise their radiation beam patterns in comparison with the standard circular piston. With the exception of the triangular surface, which has a unique characteristics, the study indicates that

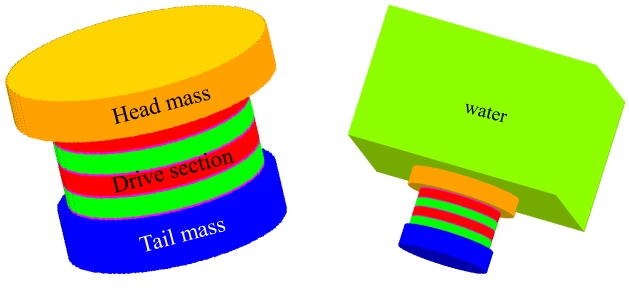

(A). Without water. (B). With water.

Figure 14. Finite element model of Tonpilz with a circular head mass diameter of 1.0λ.

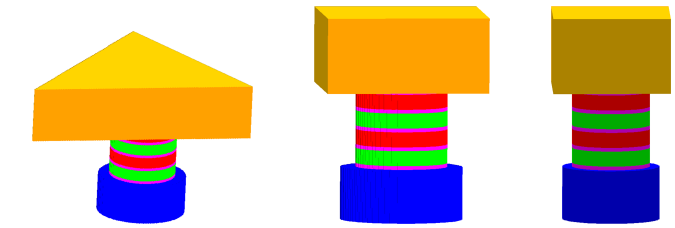

(A). Triangular. (B). Rectangular. (C). Square.

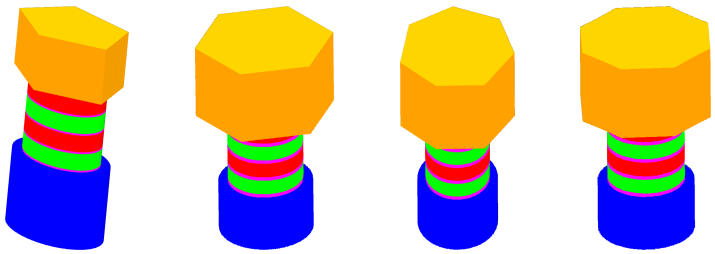

(D). Pentagonal. (E). Hexagonal. (F). Heptagonal. (G). Octagonal.

Figure 15. The finite element model of Tonpilz with head mass of different radiating polygon surfaces of equal surface areas with the circular head mass diameter of 1.0λ.

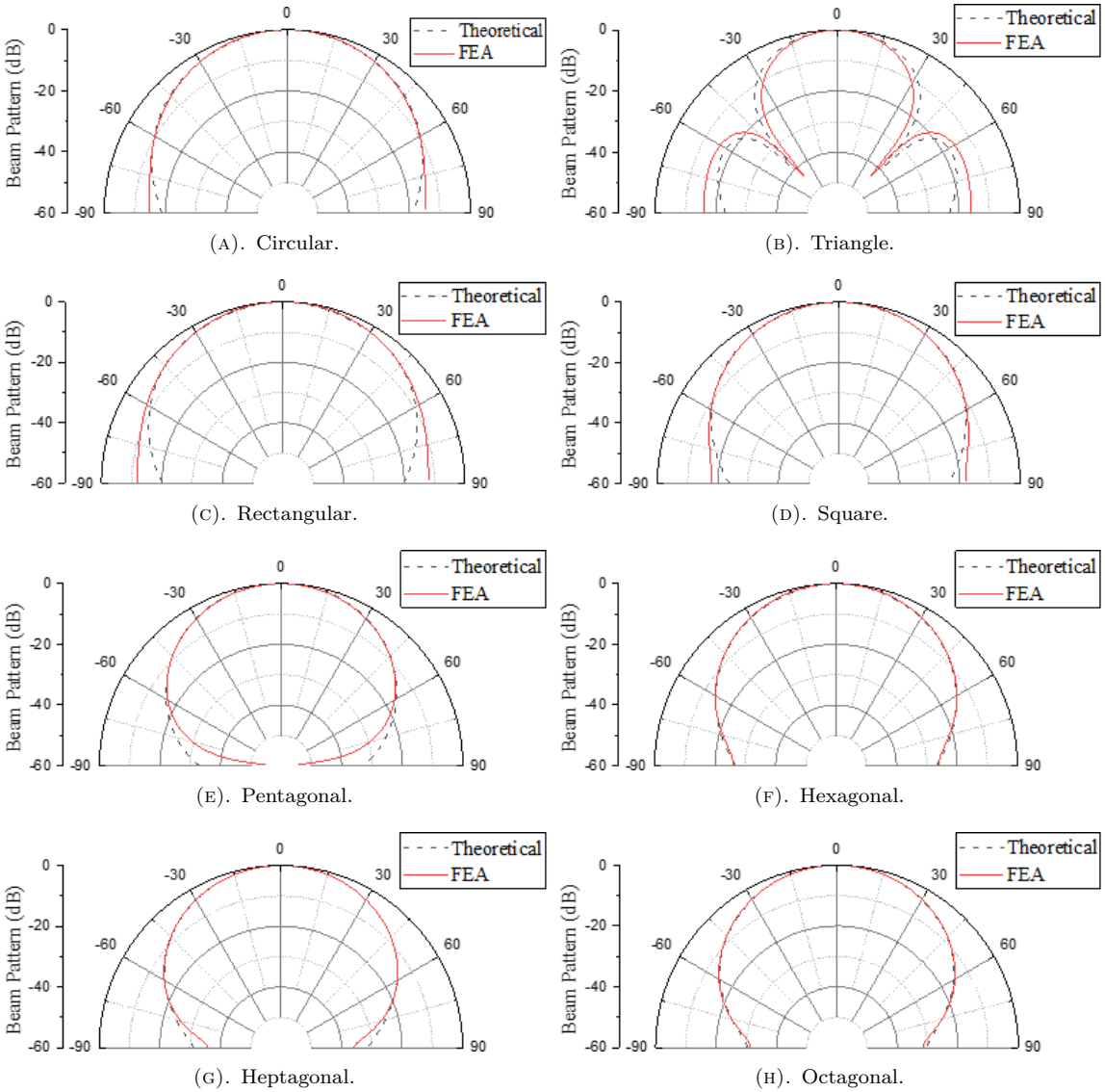

(A). Circular. (B). Triangle.

(C). Rectangular. (D). Square.

(E). Pentagonal. (F). Hexagonal.

(G). Heptagonal. (H). Octagonal.

Figure 16. The comparison between the FEA and theoretical radiation beam patterns of different polygon surfaces of acoustic piston of equal surface areas with a circular piston diameter of 1.0λ.

even-sided (symmetrical) and odd-sided (non-symmetrical) polygons, respectively, has the general directional factor of the form:

$$\left| \frac{\sin\left\{ka\tan\left(\frac{\emptyset}{2}\right)\sin\theta\right\}}{ka\tan\left(\frac{\emptyset}{2}\right)\sin\theta} \right|,$$

and:

$$\sec\left(\frac{\emptyset}{2}\right)\left[1+\left\{\frac{\sec\left(\frac{\emptyset}{2}\right)-\tan\left(\frac{\emptyset}{2}\right)}{\tan\emptyset}\right\}\right]\left[\frac{\sin\left\{ka\sec\left(\frac{\emptyset}{2}\right)\sin\theta\right\}}{ka\sec\left(\frac{\emptyset}{2}\right)\sin\theta}\right]$$
$$+\tan^3\left(\frac{\emptyset}{2}\right)\left[\frac{\sin\left\{ka\tan\left(\frac{\emptyset}{2}\right)\sin\theta\right\}}{ka\tan\left(\frac{\emptyset}{2}\right)\sin\theta}\right]$$
$$-\frac{1}{2\tan\emptyset}\left[\frac{\sin\left[ka\left\{\frac{\sec\left(\frac{\emptyset}{2}\right)+\tan\left(\frac{\emptyset}{2}\right)}{2}\right\}\sin\theta\right]}{ka\left\{\frac{\sec\left(\frac{\emptyset}{2}\right)+\tan\left(\frac{\emptyset}{2}\right)}{2}\right\}\sin\theta}\cdot\frac{\sin\left[ka\left\{\frac{\sec\left(\frac{\emptyset}{2}\right)-\tan\left(\frac{\emptyset}{2}\right)}{2}\right\}\sin\theta\right]}{ka\left\{\frac{\sec\left(\frac{\emptyset}{2}\right)-\tan\left(\frac{\emptyset}{2}\right)}{2}\right\}\sin\theta}\right],$$

where

a is the half of the side length,

ϕ is the interior angle.

All the polygons show a similar performance to a circular piston of a diameter not more than 0.28λ while the same is true for all but the triangle when the circular diameter is up to 0.43λ. In terms of the side lobe levels, the radiating beam pattern of the circular piston is better than all the polygons while all except the triangle and pentagon are identical. However, the beam width of the circular piston is lower compared to the rectangular piston and almost identical with the square piston when the circular diameter is above one wavelength. The main beam widths for the non-symmetrical polygons are relatively narrower than for the symmetrical types.

7. Conclusion

This study reveals that the perimeter and symmetry of the surface are the two factors that combine to influence the radiating beam pattern of an acoustic piston rather than the surface area or the number of sides. Hence, the symmetrical polygonal piston surface with a higher perimeter tends to have a higher beamwidth and is, therefore, most recommended in the array designs for applications where larger area coverage is desired. The major implication of this study is a more efficient array transducer configuration using the rectangle, triangle and the rest of the polygons as an alternative to the circular piston of equal surface area whose diameter is no greater than 0.5λ, 0.28λ and 0.43λ respectively. This study does not include a parallelogram in the analysis. However, it is presumed that it would have the same directional factor and exhibit the same beam pattern as the rectangle due to their nearly similar geometries.

References

[1] B.-H. Lee, J.-E. Baek, D.-W. Kim, et al. Optimized design of a sonar transmitter for the high-power control of multichannel acoustic transducers. *Electronics* **10**(21):2682, 2021. https://doi.org/10.3390/electronics10212682

[2] A. P. Sarvazyan, M. W. Urban, J. F. Greenleaf. Acoustic waves in medical imaging and diagnostics. *Ultrasound in Medicine and Biology* **39**(7):1133–1146, 2013. https://doi.org/10.1016/j.ultrasmedbio.2013.02.006

[3] V. Kumar, M. Azharudeen, C. Pothuri, K. Subramani. Heat transfer mechanism driven by acoustic body force under acoustic fields. *Physical Review Fluids* **6**:073501, 2021. https://doi.org/10.1103/PhysRevFluids.6.073501

[4] X. Wang, J. Xu, J. Ding, et al. A compact and low-frequency acoustic energy harvester using layered acoustic metamaterials. *Smart Materials and Structures* **28**(2):025035, 2019. https://doi.org/10.1088/1361-665X/aafbf6

[5] A. V. Mikhaylov, Y. L. Gobov, Y. G. Smorodinskii, G. S. Korzunin. Electromagnetic acoustic transducers for non-destructive testing of main pipelines. *Journal of Physics: Conference Series* **1636**(1):012012, 2020. https://doi.org/10.1088/1742-6596/1636/1/012012

[6] A. Agi, R. Junin, R. Shirazi, et al. Comparative study of ultrasound assisted water and surfactant flooding. *Journal of King Saud University – Engineering Sciences* **31**(3):296–303, 2019. https://doi.org/10.1016/j.jksues.2018.01.002

[7] Y. Han, X. Tian, F. Zhou, et al. A real-time 3-D underwater acoustical imaging system. *IEEE Journal of Oceanic Engineering* **39**(4):620–629, 2014. https://doi.org/10.1109/JOE.2013.2285952

[8] H. Zhou, S. H. Huang, W. Li. Parametric acoustic array and its application in underwater acoustic engineering. *Sensors* **20**(7):2148, 2020. https://doi.org/10.3390/s20072148

[9] X. Zhen-yang, W. Xin-peng, Z. Jing-yuan. Research on the directivity of transducer array based on typical array elements. *Journal of Physics: Conference Series* **1237**(4):042063, 2019. https://doi.org/10.1088/1742-6596/1237/4/042063

[10] C. Audoly. Some aspects of acoustic interactions in sonar transducer arrays. *The Journal of the Acoustical Society of America* **89**(3):1428–1433, 1991. https://doi.org/10.1121/1.400543

[11] E. E. Franco, M. A. B. Andrade, J. C. Adamowski, F. Buiochi. Acoustic beam modeling of ultrasonic transducers and arrays using the impulse response and the discrete representation methods. *Journal of the Brazilian Society of Mechanical Sciences and Engineering* **33**(4):408–416, 2011. https://doi.org/10.1590/S1678-58782011000400004

[12] N. T. Greene, G. D. Paige. Influence of sound source width on human sound localization. In *2012 Annual International Conference of the IEEE Engineering in Medicine and Biology Society*, pp. 6455–6458. 2012. https://doi.org/10.1109/EMBC.2012.6347472

[13] I. Iliev. Polar response of a circular piston. *TEM Journal* **3**(3):230–234, 2014. https://doi.org/10.18421/tem33-06

[14] T. Douglas Mast, F. Yu. Simplified expansions for radiation from a baffled circular piston. *The Journal of the Acoustical Society of America* **118**(6):3457–3464, 2005. https://doi.org/10.1121/1.2108997

[15] B. Nayak, H. Gupta, K. Roy, et al. An experimental study of the acoustic field of a single-cell piezoelectric micromachined ultrasound transducer (PMUT). In *2020 5th IEEE International Conference on Emerging Electronics (ICEE)*, pp. 1–4. 2020. https://doi.org/10.1109/ICEE50728.2020.9777041

[16] G. Zhao, K. Shi, S. Zhong. Research on array structures of acoustic directional transducer. *Mathematical Problems in Engineering* **2021**(1):6670277, 2021. https://doi.org/10.1155/2021/6670277

[17] R. Sharma, R. Agarwal, A. K. Dubey, A. Arora. Analytical modelling of hexagonal shaped capacitive micromachined ultrasonic transducer. *International Journal of System Assurance Engineering and Management* **12**(2):252–262, 2021. https://doi.org/10.1007/s13198-020-01046-y

[18] R. Sharma, R. Agarwal, A. K. Dubey, A. Arora. Optimized design of CMUT with hexagonal membranes. *International Journal of Innovative Technology and Exploring Engineering* **8**(10):1805–1809, 2019. https://doi.org/10.35940/ijitee.j9194.0881019

[19] Y. Roh, M. S. Afzal, S. R. Kwon. Analysis of the effect of radiating surface geometry on the beam pattern of underwater acoustic transducers. *Sensors and Actuators A: Physical* **330**:112843, 2021. https://doi.org/10.1016/j.sna.2021.112843

[20] Defence Research and Development Organization. Technologies for underwater surveillance systems. *Technology Focus* **25**(2):1–28, 2017.

[21] R. Rajamäki, V. Koivunen. Sparse active rectangular array with few closely spaced elements. *IEEE Signal Processing Letters* **25**(12):1820–1824, 2018. https://doi.org/10.1109/LSP.2018.2876066

[22] M.-J. Sim, C. Hong, W.-B. Jeong. Hybrid equivalent circuit/finite element/boundary element modeling for effective analysis of an acoustic transducer array with flexible surrounding structures. *Applied Sciences* **11**(6):2702, 2021. https://doi.org/10.3390/app11062702

[23] T. Yokoyama, M. Henmi, A. Hasegawa, T. Kikuchi. Effects of mutual interactions on a phased transducer array. *Japanese Journal of Applied Physics* **37**(5S):3166, 1998. https://doi.org/10.1143/JJAP.37.3166

[24] T. Beleyur. Beamshapes: a Python package to generate directivity patterns for various sound source models. *Journal of Open Source Software* **7**(69):3740, 2022. https://doi.org/10.21105/joss.03740

[25] L. E. Kinsler, A. R. Frey, A. B. Coppens, J. V. Sanders. *Fundamentals of acoustics.* John Wiley & Sons, New York, USA, 4th edn., 2000.

[26] C. Deutsch, Y. Gao. *Development of a sonar for underwater sensor platforms and surface vehicles.* Master's thesis, KTH Royal Institute of Technology Engineering Sciences, 2017.

[27] T. Mellow, L. Kärkkäinen. Expansions for the radiation impedance of a rectangular piston in an infinite baffle. *The Journal of the Acoustical Society of America* **140**(4):2867–2875, 2016. https://doi.org/10.1121/1.4964632

[28] N. Akkaya. *Acoustic radiation from baffled planar sources: A series approach.* Master's thesis, Texas Tech University, 1999.